URBAN SOCIO-SEMANTIC SEGMENTATION WITH VISION-LANGUAGE REASONING

Anonymous authors
Paper under double-blind review

ABSTRACT

As hubs of human activity, urban surfaces consist of a wealth of semantic entities. Segmenting these various entities from satellite imagery is crucial for a range of downstream applications. Current advanced segmentation models can reliably segment entities defined by physical attributes (e.g., buildings, water bodies) but still struggle with socially defined categories (e.g., schools, parks). In this work, we achieve socio-semantic segmentation by vision-language model reasoning. To facilitate this, we introduce the Urban Socio-Semantic Segmentation dataset named **SocioSeg**, a new resource comprising satellite imagery, digital maps, and pixel-level labels of social semantic entities organized in a hierarchical structure. Additionally, we propose a novel vision-language reasoning framework called **SocioReasoner** that simulates the human process of identifying and annotating social semantic entities via cross-modal recognition and multi-stage reasoning. We employ reinforcement learning to optimize this non-differentiable process and elicit the reasoning capabilities of the vision-language model. Experiments demonstrate our approach's gains over state-of-the-art models and strong zero-shot generalization. The dataset and code will be made publicly available.

1 INTRODUCTION

Urban areas, as primary hubs of human activity, are a critical subject for Earth Observation (Patino & Duque, 2013). Urban land surfaces consist of rich semantic entities, and segmenting them is crucial for downstream tasks like urban planning (Zheng et al., 2025) and environmental monitoring (Yang, 2021). These entities can be broadly grouped into two types: physical semantic entities and social semantic entities. The first encompasses entities defined by physical attributes, such as buildings, water bodies, and roads. Thanks to abundant high-resolution satellite data, current segmentation models can segment these entities precisely from visual cues in satellite imagery (Hang et al., 2022). The second comprises entities defined by social attributes, such as schools, parks, and residential districts. The identification of these entities is pivotal not only for urban analysis tasks like disease transmission (Alidadi & Sharifi, 2022), the 15-minute city (Bruno et al., 2024), but also for industrial mapping applications, such as inferring socio-semantic Areas of Interest (AOIs) from Points of Interest (POIs) to enhance navigation and recommendation (Shi et al., 2025). However, their boundaries and identities are shaped by social semantics rather than distinct visual appearances (Büttner, 2014). Since this semantic information is difficult to extract from satellite imagery alone, achieving segmentation for these socially defined entities is substantially more challenging.

Existing approaches address this challenge by incorporating auxiliary multi-modal geospatial data (e.g., Points of Interest) (Xiong et al., 2025; Zhang et al., 2017). These methods often employ separate model encoders to extract features from different modalities and train task-specific models in a fully supervised manner. However, this paradigm faces three major bottlenecks: (i) such geospatial data are often difficult to obtain due to commercial or security constraints; (ii) even when available, the heterogeneous formats and mismatched spatial granularities require complex preprocessing and alignment with satellite imagery; and (iii) because these methods are trained only on predefined categories, they can handle only a limited set of social semantic classes. These limitations underscore the need for a more versatile framework that can adeptly integrate diverse multi-modal geospatial data for socio-semantic segmentation.

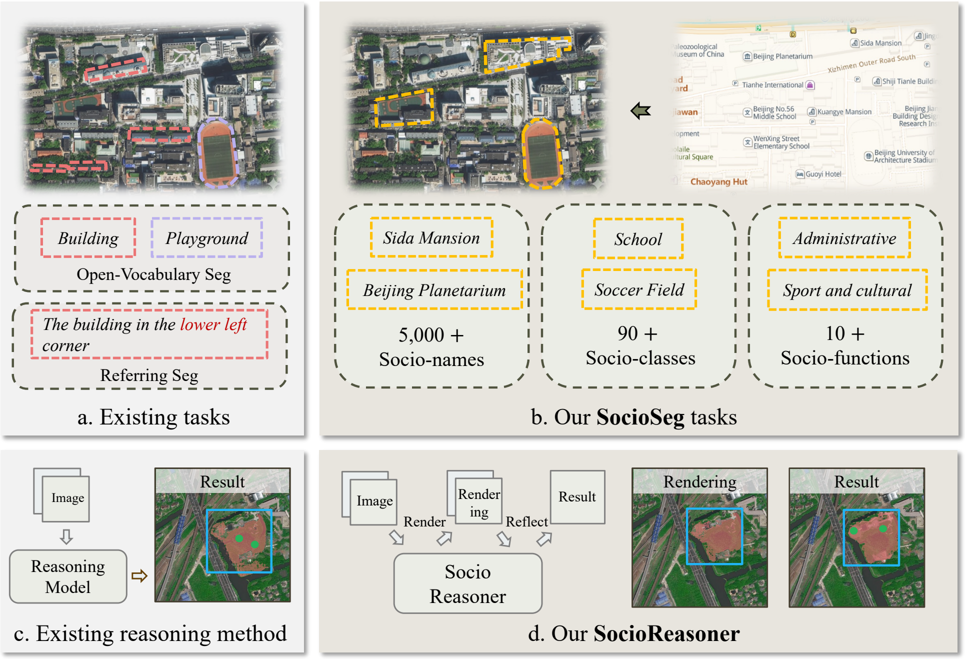

Figure 1: (a) Current works segregate physical entities. (b) Our SocioSeg identifies social entities (names, functions) via multi-modal data. (c) Existing reasoning methods employ a single-stage reasoning approach. (d) Our SocioReasoner employs a two-stage reasoning strategy with render-and-refine mechanism.

Recent advances in Vision-Language Models (VLMs) (Achiam et al., 2023; Liu et al., 2023a; Bai et al., 2025; Mall et al., 2024) offer a promising pathway toward creating such a framework. In the natural image domain, VLMs have already showcased their powerful visual understanding and reasoning capabilities on complex tasks like reasoning segmentation (Lai et al., 2024; Liu et al., 2025a; Wei et al., 2025), mathematical reasoning (Zou et al., 2024), and geolocalization (Li et al., 2024a). While some work has begun applying VLMs to satellite imagery (Li et al., 2025b; Yao et al., 2025), these efforts predominantly still focus on reasoning about physical attributes. This leaves a critical gap, as social semantics, which are inherently diverse and complex, demand precisely the sophisticated reasoning processes that VLMs excel at. This natural alignment inspires us to explore the potential of VLMs for socio-semantic segmentation.

Motivated by the aforementioned challenges and opportunities, this paper defines and tackles socio-semantic segmentation by leveraging the reasoning capabilities of VLMs. To address the critical lack of a dedicated benchmark, we introduce the Urban Socio-Semantic Segmentation dataset called **SocioSeg**. SocioSeg is structured with a three-tiered hierarchy of tasks in increasing order of complexity: (i) Socio-name segmentation (e.g., “a certain university”), (ii) Socio-class segmentation (e.g., “college”), and (iii) Socio-function segmentation (e.g., “educational”). This design means the tasks place progressively higher demands on the model’s reasoning abilities. Furthermore, to resolve the data-handling bottlenecks of previous methods, SocioSeg adopts a novel geospatial data representation paradigm. Instead of using raw geospatial data, which introduces the problems of access, alignment, and heterogeneity, SocioSeg unifies them into a digital map layer. This paradigm is highly effective: the need for protected raw data is eliminated, and the map layer is inherently spatially aligned with the satellite imagery.

Building on SocioSeg, we propose **SocioReasoner**, a vision-language reasoning framework that simulates the human process of identifying and annotating socio-semantic entities through cross-modal recognition and multi-stage reasoning. More specifically, given a textual instruction with socio-semantic concepts, SocioReasoner employs a two-stage reasoning strategy with a render-and-refine mechanism: it first generates bounding box prompts from both satellite and map imagery to localize the target region. These prompts are then fed to the Segment Anything Model (SAM) (Ravi et al., 2024) to produce an initial coarse segmentation. Recognizing that segmentation from a bounding box alone can be imprecise and inconsistent with the actual human annotation process, SocioReasoner proceeds to generate point prompts on the rendered mask to refine the boundary, ultimately generating a high-fidelity segmentation result. This entire interactive process closely mirrors the workflow of a human annotator. Since this pipeline is non-differentiable, we employ a popular reinforcement learning algorithm, GRPO (Shao et al., 2024; Guo et al., 2025), to train the framework end-to-end, which also effectively elicits the VLM's latent reasoning capabilities for the social semantic segmentation task. Extensive experiments show that our approach outperforms state-of-the-art segmentation baselines and exhibits strong zero-shot generalization capabilities, highlighting the potential of combining satellite imagery with rendered map context for social semantic understanding. In summary, our contributions are:

- We introduce socio-semantic segmentation, a novel and challenging segmentation task, and release the benchmark SocioSeg, which establishes the paradigm of rendering heterogeneous geospatial data into a unified map image, transforming a complex multi-modal challenge into a visual reasoning task.
- We propose SocioReasoner, a segmentation framework that mimics human annotation via a multi-stage reasoning process. This non-differentiable workflow is optimized using reinforcement learning with a dedicated reward function, effectively eliciting the model's reasoning capabilities.
- Extensive empirical evidence demonstrates the effectiveness and generalization capabilities of our approach, highlighting its potential for real-world applications.

2 Related Work

2.1 Semantic Segmentation

Semantic segmentation is a fundamental task in computer vision (Voulodimos et al., 2018). Early deep learning methods trained models in a fully supervised manner, enabling them to recognize only a predefined set of semantic categories (Ronneberger et al., 2015; Xie et al., 2021). With the advancement of pre-trained models, tasks such as open-vocabulary segmentation (Ghiasi et al., 2022) and referring segmentation (Wang et al., 2022) have emerged, allowing models to identify unseen categories or segment objects based on textual descriptions. More recently, the task of reasoning segmentation (Lai et al., 2024) is introduced, where the input text describes the target's function or relationship rather than its visual appearance. This demands more sophisticated reasoning capabilities from the model. Notably, a significant body of current work now employs VLM-based paradigms to address reasoning segmentation tasks (Liu et al., 2025a; You & Wu, 2025; Liu et al., 2025b). These methods feed visual prompts (e.g., bounding boxes or points) derived from VLM inference into the SAM to perform segmentation, and employ reinforcement learning to elicit the model's reasoning capabilities.

Semantic segmentation from satellite imagery follows a similar developmental trajectory (Kotaridis & Lazaridou, 2021). It began with fully supervised models for extracting features like buildings (Cheng et al., 2019) and roads (Sun et al., 2019), and has since progressed to explorations in open-vocabulary (Li et al., 2025a; Zhu et al., 2025) and referring segmentation (Chen et al., 2025). Recently, some studies also begin to tackle reasoning segmentation on satellite imagery, often by using closed-source vision language model to re-frame existing segmentation categories into text that requires reasoning (Li et al., 2025b). This existing work predominantly focuses on categories defined by physical attributes (e.g., buildings, water bodies) or categories with distinct visual features. Socio-semantic categories (e.g., schools, parks), whose boundaries and identities are determined more by social constructs than by distinct visual cues, remain a significant challenge for methods that rely solely on satellite imagery. In contrast to existing work, our paper specifically targets these socio-semantic categories within urban regions.

2.2 Multi-Modal Approaches for Urban Understanding

The task of segmenting urban social semantic entities, which we term urban socio-semantic segmentation, is a nascent research area. While no prior work directly addresses this task, related problems exist in the field of urban science, such as land-use classification (Xiong et al., 2025) and urban functional zone (Yao et al., 2018). These studies typically fuse multimodal data, such as Points of

Interest (POIs) and road networks, with satellite imagery. Their common approach involves using separate model encoders for different data modalities and then merging the extracted features for classification or segmentation (Xiong et al., 2025; Zhang et al., 2017). However, these methods, which rely on raw multi-modal data, face several critical bottlenecks. They are often hampered by challenges in data acquisition (due to commercial or security constraints), the complexity of handling heterogeneous data formats and mismatched spatial granularities, and an inability to generalize beyond a limited set of predefined categories. Crucially, this highlights the fundamental difference between our task and traditional land-use classification. While the latter typically targets a fixed, closed set of categories, our socio-semantic segmentation involves fine-grained attributes (over 90 categories) and specific entity names, where each instance acts as a unique class. Consequently, our task aligns more closely with open-vocabulary, referring, or reasoning segmentation rather than standard classification.

3 SocioSeg Dataset

Existing semantic segmentation dataset (Wang et al., 2021; Li et al., 2024b) from satellite imagery has been largely confined to extracting entities defined by physical attributes. To expand the scope to social semantics, we introduce the SocioSeg dataset, which is distinguished by two key features:

Hierarchical Socio-Semantic Segmentation Task Design. As illustrated in Appendix A.1.1, Figure 6, we define urban socio-semantic entities across three hierarchical levels of increasing abstraction and difficulty: Socio-names (e.g., “a certain university”), Socio-classes (e.g., “college”), and Socio-functions (e.g., “educational”). This tiered structure facilitates a progressive evaluation of a model’s reasoning capabilities. Above all, SocioSeg is exceptionally rich in social semantic information, containing over 5,000 Socio-names, 90 Socio-classes, and 10 Socio-functions.

Multi-Modal Data with Digital Map Representation. A key innovation of the SocioSeg dataset is its unification of diverse geospatial information into a single digital map layer. This representation offers several distinct advantages. First, it overcomes data accessibility issues, as publicly available map layers replace raw multi-modal data that are often proprietary or restricted. Second, the map layer is inherently co-registered with the satellite imagery, which eliminates the need for complex data alignment. Finally, this fusion into a single visual modality provides rich socio-semantic cues that are crucial for enhancing a model’s social reasoning capabilities.

We construct the inputs for SocioSeg by sourcing satellite images and digital maps from the Amap public API[1], which provides these maps in both Chinese and English versions. The digital maps render only basic geospatial information, including roads and points of interest. We then collected the ground-truth socio-semantic labels for the corresponding regions. (Further details on the annotation procedure and dataset statistics are available in Appendix A.1.1). As a result, the SocioSeg dataset comprises over 13,000 samples distributed across the three hierarchical tasks. Each sample consists of a satellite image, a digital map, and a corresponding socio-semantic mask label. We partitioned the dataset into training, validation, and test sets using a 6:1:3 ratio, ensuring that the sample counts and class distributions for each hierarchical task are consistent across all splits.

4 SocioReasoner Framework

4.1 Human-Like Reasoning Segmentation Process

Prevailing reasoning-segmentation methods (Liu et al., 2025b; Yao et al., 2025) typically follow a single-stage pipeline: a Vision-Language Model (VLM) generates visual prompts (e.g., a bounding box), which are then fed into a frozen SAM to produce the final mask. Because the weights of SAM are fixed, these methods lack direct control over the output quality, often resulting in coarse or inaccurate segmentation. In contrast, our SocioReasoner framework (as shown in Figure 2) employs a two-stage reasoning strategy with a render-and-refine mechanism to emulate the sequential workflow of a human annotator. This multi-stage approach enhances precision and makes the model’s inference steps transparent and interpretable.

[1] Amap API Documentation. https://lbs.amap.com/. Accessed: 2025-05-14.

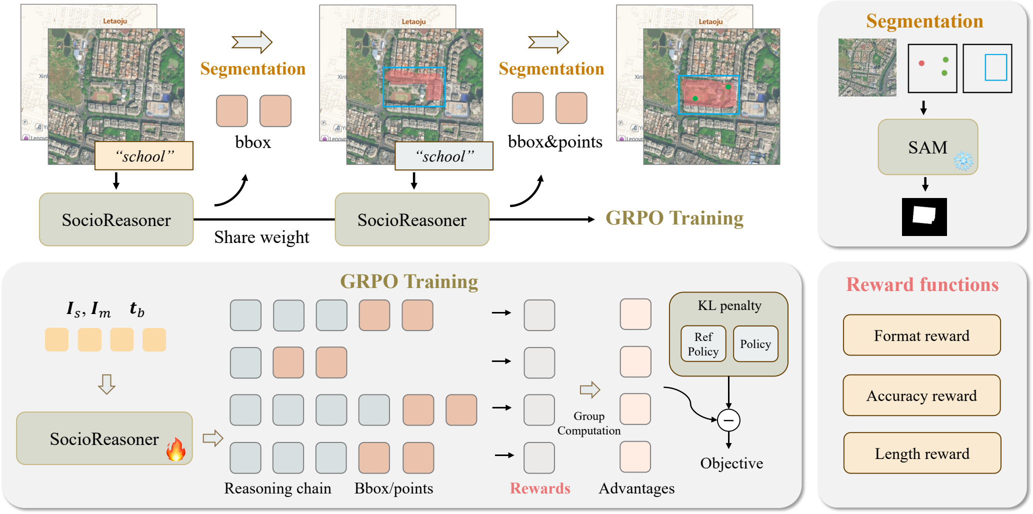

Figure 2: SocioReasoner Framework. Given a satellite image, a digital map, and a textual instruction, the VLM first generates bounding boxes to localize candidate regions. These boxes are fed into SAM to produce a coarse mask. The boxes and mask are then rendered onto the inputs for re-evaluation. The VLM emits boxes and points, which are again fed into SAM to yield the final mask.

Stage-1 (Localization): Emitting a set of 2D bounding boxes. Let the VLM be denoted by $\mathcal{F}$. Given a satellite image $\mathbf{I}_s$, a digital map $\mathbf{I}_m$, and a textual instruction $\mathbf{t}_b$, the VLM emits a set of 2D bounding boxes $\mathcal{B} = \{\mathbf{b}_i\}_{i=1}^{N}$ to localize candidate target regions:

$$\mathcal{B} = \mathcal{F}(\mathbf{I}_s, \mathbf{I}_m, \mathbf{t}_b). \tag{1}$$

These bounding boxes are supplied to a pre-trained segmentation model, SAM ($\mathcal{S}$) (Ravi et al., 2024), to produce a preliminary coarse mask $\mathbf{M}_c$:

$$\mathbf{M}_c = \mathcal{S}(\mathbf{I}_s, \text{prompt} = \mathcal{B}). \tag{2}$$

Stage-2 (Refinement): Emitting both a set of bounding boxes and points. Recognizing that segmentation from bounding boxes alone can be imprecise, we provide visual feedback to the VLM by rendering both the boxes and the coarse mask onto the inputs. A rendering function $\mathcal{D}$ overlays $\mathcal{B}$ and $\mathbf{M}_c$ onto the satellite image $\mathbf{I}_s$ and the digital map $\mathbf{I}_m$, producing a pair of rendered images $(\mathbf{I}_{s,r}, \mathbf{I}_{m,r})$ for re-evaluation:

$$\mathbf{I}_{s,r} = \mathcal{D}(\mathbf{I}_s, \mathcal{B}, \mathbf{M}_c), \quad \mathbf{I}_{m,r} = \mathcal{D}(\mathbf{I}_m, \mathcal{B}, \mathbf{M}_c). \tag{3}$$

Conditioned on $(\mathbf{I}_{s,r}, \mathbf{I}_{m,r})$ and the instruction $\mathbf{t}_p$, the VLM emits a set of bounding boxes $\mathcal{B}$ together with points $\mathcal{P} = \{\mathbf{p}_j\}_{j=1}^{K}$:

$$\{\mathcal{B}, \mathcal{P}\} = \mathcal{F}(\mathbf{I}_{s,r}, \mathbf{I}_{m,r}, \mathbf{t}_p). \tag{4}$$

Finally, the comprehensive set of prompts (bounding boxes and points) is fed back into SAM to yield the final mask $\mathbf{M}_f$:

$$\mathbf{M}_f = \mathcal{S}(\mathbf{I}_s, \text{prompt} = \{\mathcal{B}, \mathcal{P}\}). \tag{5}$$

By decomposing the segmentation challenge into this sequence of localization and refinement, SocioReasoner achieves superior accuracy and provides an explicit reasoning chain. As this entire pipeline is non-differentiable, we leverage reinforcement learning to optimize the VLM's policy for generating these sequential prompts.

4.2 End to End Reinforcement Learning Optimization

We optimize the non-differentiable, multi-stage prompting policy of SocioReasoner using reinforcement learning with Group Relative Policy Optimization (GRPO) (Guo et al., 2025). A single Vision-Language Model (VLM) policy is shared across both stages and emits structured textual outputs that encode prompts for SAM. The environment parses these outputs, executes SAM with the parsed prompts, and returns a scalar reward.

Stage-1 (Localization) Optimization. Given an input $\mathbf{x}_1 = (\mathbf{I}_s, \mathbf{I}_m, \mathbf{t}_b)$, the policy π_θ stochastically generates a completion $\mathbf{y}_1$ that encodes a set of bounding boxes. The environment parses $\mathbf{y}_1$ to obtain $\mathcal{B}$, runs SAM to produce a coarse mask $\mathbf{M}_c$, and returns a stage-1 reward $R_1(\mathbf{y}_1; \mathbf{x}_1)$ comprising: (i) a binary syntax reward to ensure valid JSON output, (ii) a localization accuracy term for the predicted boxes, and (iii) a reward for matched object count. GRPO is applied per input by drawing G completions $\{\mathbf{y}_1^{(g)}\}_{g=1}^{G}$, computing rewards $\{R_1^{(g)}\}_{g=1}^{G}$, and defining a group-relative baseline $b_1(\mathbf{x}_1) = \frac{1}{G}\sum_{g=1}^{G} R_1^{(g)}$, with advantages $A_1^{(g)} = R_1^{(g)} - b_1(\mathbf{x}_1)$. The stage-1 objective is a clipped PPO-like surrogate with KL regularization against a frozen reference policy π_{ref}:

$$\begin{aligned} \mathcal{L}_1(\theta) \;=\; & -\frac{1}{G}\sum_{g=1}^{G} \sum_{t \in \mathcal{I}(\mathbf{y}_1^{(g)})} \min\Big(r_{1,t}^{(g)} A_1^{(g)},\; \text{clip}\big(r_{1,t}^{(g)}, 1-\epsilon, 1+\epsilon\big) A_1^{(g)} \Big) \\ & +\; \beta\, \text{KL}\big(\pi_\theta(\cdot|\mathbf{x}_1) \,\|\, \pi_{\text{ref}}(\cdot|\mathbf{x}_1)\big), \end{aligned} \tag{6}$$

where $r_{1,t}^{(g)} = \frac{\pi_\theta\left(y_{1,t}^{(g)} \mid y_{1,<t}^{(g)}, \mathbf{x}_1\right)}{\pi_{\theta_{\text{old}}}\left(y_{1,t}^{(g)} \mid y_{1,<t}^{(g)}, \mathbf{x}_1\right)}$ is the token-level importance ratio. The hyperparameters ϵ and β control the PPO clipping and KL regularization, respectively.

Stage-2 (Refinement) Optimization. Conditioned on the rendered visual feedback and the coarse mask, the policy refines the prompts. We construct $\mathbf{x}_2 = (\mathbf{I}_{s,r}, \mathbf{I}_{m,r}, \mathbf{t}_p, \mathbf{M}_c)$ by overlaying the stage-1 boxes and coarse mask using the renderer $\mathcal{D}$. The policy π_θ emits $\mathbf{y}_2$ that encodes bounding boxes and points. The environment parses $\mathbf{y}_2$ to obtain $\{\tilde{\mathcal{B}}, \mathcal{P}\}$, runs SAM to produce the final mask $\mathbf{M}_f$, and returns a stage-2 reward $R_2(\mathbf{y}_2; \mathbf{x}_2)$ comprising: (i) a binary syntax reward for valid JSON, (ii) a pixel-level IoU term for $\mathbf{M}_f$, and (iii) a reward for point length. GRPO sampling, baseline/advantage computation, and the clipped surrogate with KL regularization follow the same formulation as in stage-1.

Training Schedule. Within a single reinforcement learning step, we execute both stages sequentially: (i) sample, evaluate, and update with $\mathcal{L}_1(\theta)$ using stage-1 rollouts; (ii) construct the stage-2 inputs from the stage-1 outputs, then sample, evaluate, and update with $\mathcal{L}_2(\theta)$. This two-stage procedure aligns optimization with the sequential localization–refinement workflow. Detailed formulations of the rewards R_1 and R_2 are provided in the Appendix A.2.2. The overall training algorithm is summarized in Algorithm 1.

5 Experiments

5.1 Baselines and Evaluation Metrics

We primarily compare against three families of methods: (i) standard semantic segmentation models, including the CNN-based UNet (Ronneberger et al., 2015) and the Transformer-based SegFormer (Xie et al., 2021); (ii) state-of-the-art reasoning segmentation for natural images, including VisionReasoner (Liu et al., 2025b), Seg-R1 (You & Wu, 2025), and SAM-R1 (Huang et al., 2025); (iii) state-of-the-art satellite image segmentation methods, including the open-vocabulary segmentation SegEarth-OV (Li et al., 2025a), referring segmentation RSRefSeg (Chen et al., 2025), and reasoning-based approaches SegEarth-R1 (Li et al., 2025b) and RemoteReasoner (Yao et al., 2025). Because SocioSeg provides two images (satellite and digital map), we adapt all VLM-based baselines to accept dual-image inputs; for methods (RSRefSeg and SegEarth-R1) that do not support multiple images, we provide only the satellite image. *All baselines are re-trained on the SocioSeg training split to ensure fair comparison.* Additionally, given the challenging nature of the SocioSeg

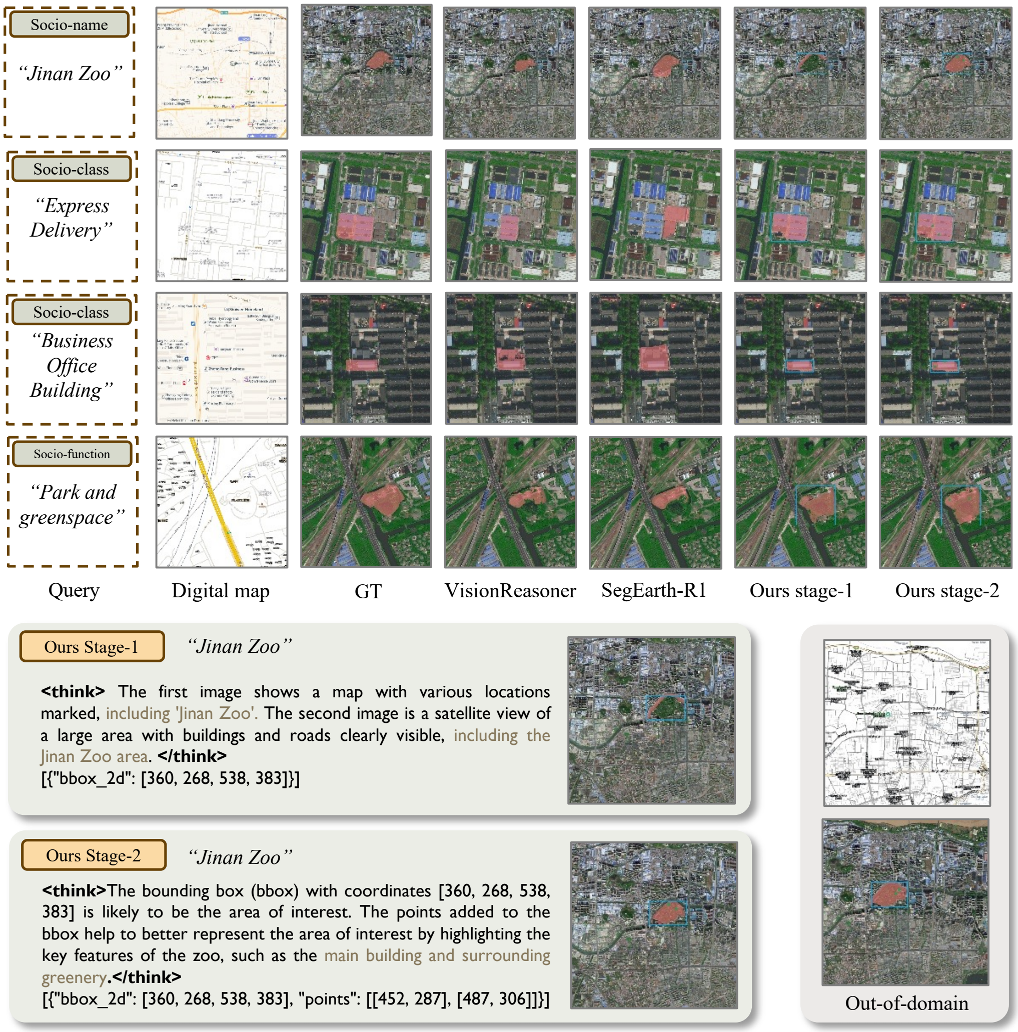

<think> The first image shows a map with various locations marked, including 'Jinan Zoo'. The second image is a satellite view of a large area with buildings and roads clearly visible, including the Jinan Zoo area. **</think>**
[{"bbox_2d": [360, 268, 538, 383]}]

<think>The bounding box (bbox) with coordinates [360, 268, 538, 383] is likely to be the area of interest. The points added to the bbox help to better represent the area of interest by highlighting the key features of the zoo, such as the main building and surrounding greenery.**</think>**
[{"bbox_2d": [360, 268, 538, 383], "points": [[452, 287], [487, 306]]}]

Figure 3: Visualization of the SocioReasoner results. The top panel shows a comparison between the results of SocioReasoner (with both stages visualized) and competitive baselines. The bottom-left panel illustrates the reasoning process of SocioReasoner. The bottom-right panel displays the visualization results of SocioReasoner on the out-of-domain dataset.

benchmark, we employ off-the-shelf Large Multimodal Models as reference models to provide a more comprehensive evaluation. Detailed experimental results for these models are provided in the Appendix A.4. For evaluation, we follow previous work (Lai et al., 2024) in reporting cIoU and gIoU. Additionally, we employ the F1 score to assess instance-level performance.

5.2 Comparison with State-of-the-Art Methods

Comparison with state-of-the-art methods on the SocioSeg test set is presented in Figure 3 and Appendix A.6. The quantitative results are presented in Table 1, with results grouped by task for clarity. Our SocioReasoner framework consistently outperforms all baselines across all three hierarchical tasks, demonstrating its effectiveness in handling the complexities of socio-semantic segmentation. This performance gain underscores the advantage of our human-like reasoning process and the use of rendered map context in enhancing the model's understanding of social semantics. However, because SocioReasoner simulates a multi-step human reasoning process, its inference time is longer compared to other methods. We provide a detailed analysis of SocioReasoner's inference time in Appendix A.5.2. Additionally, we illustrate the accuracy for individual Socio-classes in Figure 4,

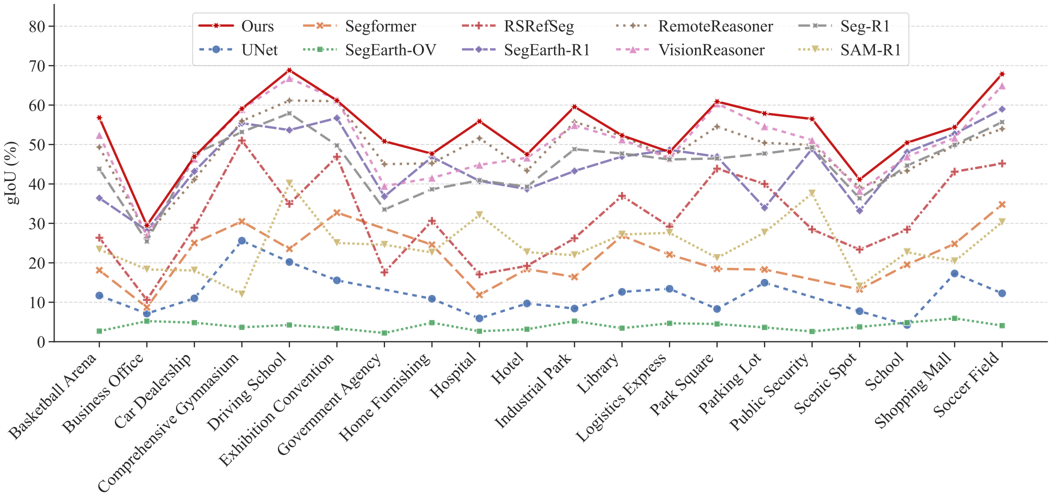

Figure 4: Per-class accuracy comparison across Socio-classes. We select the top-20 most frequent classes in the test set for visualization. The full results are available in Appendix A.5.1.

demonstrating that our method maintains strong competitiveness across the top-20 most frequent classes. The accuracy metrics and detailed analysis for all classes are provided in Appendix A.5.1.

Comparison with standard semantic segmentation methods. Since standard semantic segmentation models are incapable of processing multimodal inputs, they fail to perceive the social semantic information inherent in the SocioSeg task. Consequently, under this setting, the task for standard models degenerates into a binary classification problem. As observed, UNet and SegFormer exhibit inferior performance on SocioSeg compared to the other two categories of methods, whereas our approach significantly outperforms them.

Comparison with natural image reasoning segmentation methods. Similar to SocioReasoner, VisionReasoner, Seg-R1, and SAM-R1 all support multi-image inputs and therefore perform relatively well on SocioSeg. Notably, SAM-R1 (Huang et al., 2025) lacks constraints on the length of the output point prompts; in our reproduction, it emits a large number of point coordinates, which degrades performance. These methods freeze SAM parameters and perform single-stage inference. In contrast, our SocioReasoner framework surpasses these methods by a notable margin across all metrics. This improvement is attributable to our multi-stage reasoning process that mimics human annotation, providing reflection and refinement capabilities that lead to more accurate segmentation.

Comparison with advanced satellite image segmentation methods. SegEarth-OV completely freezes the CLIP encoder, limiting its recognition capabilities to the categories present in CLIP's pre-training data. Since SocioSeg features novel semantic categories related to social attributes, this method fails to function effectively on the SocioSeg task. RSRefSeg and SegEarth-R1, which are designed for segmenting physical attributes and support only a single satellite image input, show limited performance on socio-semantic tasks. However, because they are trained in a fully supervised manner without freezing the mask decoder, they achieve some performance gains. In contrast, our approach leverages multimodal reasoning, effectively integrating satellite imagery with digital map context to capture nuanced social semantics. RemoteReasoner adopts a design similar to VisionReasoner, supports multi-image inputs, and performs well on SocioSeg. Our SocioReasoner framework outperforms RemoteReasoner, highlighting the benefits of our two-stage localization and refinement process, which enables more precise segmentation through iterative reasoning.

5.3 Ablation Studies

We ablate three core design choices of SocioReasoner: the training/inference scheme (single-stage vs. two-stage), the impact of reinforcement learning (RL), and the number of points issued in the second stage. Results are summarized in Table 2, Table 3, and Table 4. The full results of each ablation setting are provided in Appendix A.5.2.

Method	Socio-name			Socio-class			Socio-function			All dataset		
	cIoU	gIoU	F1	cIoU	gIoU	F1	cIoU	gIoU	F1	cIoU	gIoU	F1
UNet	10.9	9.4	8.0	12.6	11.9	11.2	11.1	10.6	10.4	11.7	10.7	10.0
Segformer	22.0	19.6	18.1	22.4	21.4	19.5	21.4	20.2	17.9	22.1	20.5	18.7
VisionReasoner	48.5	50.9	58.4	44.4	49.3	55.5	36.3	41.8	45.0	44.0	48.5	54.3
Seg-R1	46.0	48.1	50.4	40.4	44.7	45.2	34.5	39.5	36.5	41.0	45.0	45.2
SAM-R1	25.6	25.4	37.2	22.3	23.8	32.1	17.7	19.9	25.2	22.5	23.7	32.4
SegEarth-OV	3.3	3.3	0.0	3.8	3.8	0.0	4.2	4.2	0.0	3.7	3.7	0.0
RSRefSeg	27.1	25.4	30.9	30.7	30.6	35.3	28.7	28.8	30.8	29.0	28.3	32.8
SegEarth-R1	36.9	42.1	46.9	38.9	45.1	50.0	39.5	45.6	47.4	38.3	44.1	48.4
RemoteReasoner	46.6	49.5	56.1	42.9	48.0	53.9	38.0	43.5	47.2	43.2	47.7	53.3
Ours	**52.6**	**55.7**	**64.6**	**47.6**	**52.8**	**60.1**	**40.6**	**46.9**	**50.3**	**47.9**	**52.8**	**59.7**

Table 1: Comparison with state-of-the-art methods on SocioSeg test set, split by task groups for readability. The best performance in each column is highlighted in **bold**. The second best is underlined. Baselines are re-trained on the SocioSeg training split to ensure fair comparison.

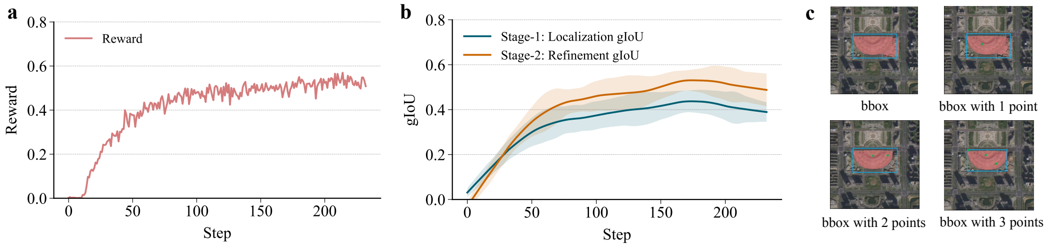

Figure 5: (a) Sum reward during training. It shows the sum of rewards across training steps in the two-stage workflow. (b) Multi-stage gIoU during training. It shows the gIoU improvement across training steps in the two-stage workflow. (c) Different number of points. It visualizes the result of SocioReasoner in the refinement stage with different numbers of points.

Impact of the training/inference scheme. In the "w/o reflection" configuration, the model bypasses the two-stage workflow and instead produces bounding boxes and points in a single stage, equivalent to VisionReasoner's one-step prompting. This setting performs the worst for two reasons: (i) without an iterative process, the model cannot self-correct after observing the coarse mask; and (ii) it must solve a complex planning-and-parsing problem in one shot (jointly synthesizing boxes and points in a long structured output), which increases failure rates. In the "w/o refinement" ablation, we use the model trained with the two-stage pipeline but halt the inference process after Stage-1. The output from this initial localization stage is used directly as the final result, completely bypassing the refinement stage. The complete pipeline ("Ours"), which overlays stage-1 outputs and emits both boxes and points, achieves the best results. Figure 5b shows the evolution of mask IoU across the two stages during RL training: stage-1 accuracy is initially higher because the model focuses more on localization early on; as training progresses, the model increasingly leverages points to improve the mask, leading to a steady rise in stage-2 accuracy. This finding highlights the effectiveness of our multi-stage reasoning process, where the refinement stage contributes to enhancing segmentation quality.

Impact of the number of points in the refinement stage. In our reward function, the parameter μ directly controls the number of point prompts generated in the refinement stage. We present the experimental results for different numbers of points in Table 3 and visualize the corresponding qualitative results in Figure 5c. We observe that a single point prompt often fails to cover the entire target, while the model struggles to learn a stable distribution for three points, with marginal performance gains compared to using two. Therefore, we select two points as the final design choice.

Impact of the RL. Figure 5a illustrates the reward trajectory during training. The consistent upward trend demonstrates that RL effectively optimizes SocioReasoner's human-like workflow. To further demonstrate the effectiveness of our training strategy, we compare SocioReasoner trained via RL

Table 2: Ablation of multi-stage design.

Method	All dataset		
	cIoU	gIoU	F1
w/o reflection	44.0	48.5	54.3
w/o refinement	46.4	50.8	57.5
Ours	**47.9**	**52.8**	**59.7**

Table 3: Ablation of point number.

Method	All dataset		
	cIoU	gIoU	F1
1 point refinement	47.6	51.2	58.0
2 points refinement	47.9	**52.8**	**59.7**
3 points refinement	**48.9**	52.3	58.8

Table 4: Generalization of SocioReasoner, where ID and OOD refer to in-domain and out-of-domain, respectively.

Method	ID			OOD (Map Style)			OOD (New Region)		
	cIoU	gIoU	F1	cIoU	gIoU	F1	cIoU	gIoU	F1
VisionReasoner (SFT)	44.1	47.2	52.1	38.8	40.9	45.5	22.5	24.7	26.1
VisionReasoner (RL)	44.0	48.5	54.3	42.0	44.4	51.2	32.8	34.4	35.0
Ours (SFT)	47.1	51.4	57.8	39.7	42.0	46.9	30.1	32.3	31.5
Ours (RL)	**47.9**	**52.8**	**59.7**	**45.1**	**49.1**	**57.7**	**40.2**	**43.4**	**42.9**

against a Supervised Fine-Tuning (SFT) baseline. We evaluate performance not only on the in-domain (ID) Amap data but also on two challenging out-of-domain (OOD) scenarios using Google Maps tiles, as reported in Table 4. The "OOD (Map Style)" setting tests robustness to cartographic style shifts. Furthermore, we introduce a specific "OOD (New Region)" setting evaluated on a newly constructed dataset sampled from five global cities: Tokyo (Asia), New York (North America), São Paulo (South America), London (Europe), and Nairobi (Africa). This dataset, which is detailed in Appendix A.1.2, comprises 3,200 samples covering 80 categories, including 24 novel classes unseen during training. While the SFT baseline suffers significant performance degradation on these OOD tasks, our RL method maintains high robustness, achieving superior results on the diverse regional dataset. A similar trend is observed in the VisionReasoner baseline, where the RL-optimized version consistently outperforms the SFT variant, further corroborating the efficacy of RL in enhancing reasoning capabilities. This indicates that minimizing the RL objective, which directly optimizes the non-differentiable IoU, enables the model to learn more generalized geometric reasoning policies that transfer effectively across different map styles and geographic regions.

6 Conclusion

This paper introduces the task of urban socio-semantic segmentation and present SocioSeg, the first benchmark for this challenge. SocioSeg's key contribution is a new paradigm that renders heterogeneous geospatial data into a unified map, transforming a complex multi-modal problem into a visual reasoning task. We also propose SocioReasoner, a framework that leverages Vision-Language Models to mimic the human annotation process through a multi-stage reasoning segmentation workflow. By optimizing this non-differentiable pipeline with reinforcement learning, we effectively elicit the model's latent reasoning capabilities. Extensive experiments demonstrate that our approach outperforms existing methods and exhibits strong zero-shot generalization to unseen map sources. Our work highlights the potential of VLM reasoning for complex geospatial analysis.

Ethics Statement Our research utilizes publicly accessible satellite and map data, specifically from the Amap public API, for the creation of the SocioSeg dataset. The manual annotation process was confined to identifying and labeling public and private functional zones without collecting or inferring any personally identifiable information (PII). We strongly advocate for the responsible deployment of our model, urging users to consider the societal impact and to prevent applications that could lead to surveillance or discriminatory outcomes.

Reproducibility Statement To ensure the full reproducibility of our findings, we have provided comprehensive implementation details throughout the paper. The construction and statistics of our SocioSeg benchmark are detailed in Sec 3 and Appendix A.1. The architecture of the SocioReasoner framework, including the multi-stage reasoning process, is described in Sec 4.1. Key details for the reinforcement learning optimization, including the reward function design and GRPO training algorithm, are presented in Sec 4.2 and Appendix A.2. In line with our commitment to open science, the SocioSeg dataset and source code will be made publicly available.

LLM clarification We clarify the use of Large Language Models (LLMs) in the preparation of this manuscript. Specifically, LLMs were employed for two main purposes: translation of initial drafts from our native language and subsequent language polishing. This process involved correcting grammatical errors, improving sentence structure, and enhancing the overall readability and flow of the text. It is crucial to emphasize that all core scientific content, intellectual contributions, and original ideas presented in this paper are exclusively the work of the human authors. This includes the formulation of the research problem, the development of the SocioReasoner framework, the creation of the SocioSeg dataset, the experimental design, and the analysis of the results. The LLM served strictly as a writing aid and was not involved in any conceptual or analytical aspect of this research.

REFERENCES

Josh Achiam, Steven Adler, Sandhini Agarwal, Lama Ahmad, Ilge Akkaya, Florencia Leoni Aleman, Diogo Almeida, Janko Altenschmidt, Sam Altman, Shyamal Anadkat, et al. Gpt-4 technical report. *arXiv preprint arXiv:2303.08774*, 2023.

Mehdi Alidadi and Ayyoob Sharifi. Effects of the built environment and human factors on the spread of covid-19: A systematic literature review. *Science of The Total Environment*, 850:158056, 2022. ISSN 0048-9697.

Shuai Bai, Keqin Chen, Xuejing Liu, Jialin Wang, Wenbin Ge, Sibo Song, Kai Dang, Peng Wang, Shijie Wang, Jun Tang, et al. Qwen2. 5-vl technical report. *arXiv preprint arXiv:2502.13923*, 2025.

Matteo Bruno, Hygor Piaget Monteiro Melo, Bruno Campanelli, and Vittorio Loreto. A universal framework for inclusive 15-minute cities. *Nature Cities*, 1:633–641, 2024.

György Büttner. *CORINE Land Cover and Land Cover Change Products*, pp. 55–74. Springer Netherlands, Dordrecht, 2014. ISBN 978-94-007-7969-3.

Keyan Chen, Jiafan Zhang, Chenyang Liu, Zhengxia Zou, and Zhenwei Shi. Rsrefseg: Referring remote sensing image segmentation with foundation models. In *2025 IEEE International Geoscience and Remote Sensing Symposium (IGARSS)*. IEEE, 2025.

Dominic Cheng, Renjie Liao, Sanja Fidler, and Raquel Urtasun. Darnet: Deep active ray network for building segmentation. In *Proceedings of the IEEE/CVF conference on computer vision and pattern recognition*, pp. 7431–7439, 2019.

Golnaz Ghiasi, Xiuye Gu, Yin Cui, and Tsung-Yi Lin. Scaling open-vocabulary image segmentation with image-level labels. In *European conference on computer vision*, pp. 540–557. Springer, 2022.

Peng Gong, Bin Chen, Xuecao Li, Han Liu, Jie Wang, Yuqi Bai, Jingming Chen, Xi Chen, Lei Fang, Shuailong Feng, et al. Mapping essential urban land use categories in china (euluc-china): Preliminary results for 2018. *Science Bulletin*, 65(3):182–187, 2020.

Daya Guo, Dejian Yang, Haowei Zhang, Junxiao Song, Ruoyu Zhang, Runxin Xu, Qihao Zhu, Shirong Ma, Peiyi Wang, Xiao Bi, et al. Deepseek-r1: Incentivizing reasoning capability in llms via reinforcement learning. *arXiv preprint arXiv:2501.12948*, 2025.

Xin Guo, Jiangwei Lao, Bo Dang, Yingying Zhang, Lei Yu, Lixiang Ru, Liheng Zhong, Ziyuan Huang, Kang Wu, Dingxiang Hu, et al. Skysense: A multi-modal remote sensing foundation model towards universal interpretation for earth observation imagery. In *Proceedings of the IEEE/CVF Conference on Computer Vision and Pattern Recognition*, pp. 27672–27683, 2024.

Renlong Hang, Ping Yang, Feng Zhou, and Qingshan Liu. Multiscale progressive segmentation network for high-resolution remote sensing imagery. *IEEE Transactions on Geoscience and Remote Sensing*, 60:1–12, 2022.

Yunfeng Hu and Yueqi Han. Identification of urban functional areas based on poi data: A case study of the guangzhou economic and technological development zone. *Sustainability*, 11(5): 1385, 2019.

Jiaqi Huang, Zunnan Xu, Jun Zhou, Ting Liu, Yicheng Xiao, Mingwen Ou, Bowen Ji, Xiu Li, and Kehong Yuan. Sam-r1: Leveraging sam for reward feedback in multimodal segmentation via reinforcement learning. In *Advances in Neural Information Processing Systems*, 2025.

Ioannis Kotaridis and Maria Lazaridou. Remote sensing image segmentation advances: A meta-analysis. *ISPRS Journal of Photogrammetry and Remote Sensing*, 173:309–322, 2021.

Xin Lai, Zhuotao Tian, Yukang Chen, Yanwei Li, Yuhui Yuan, Shu Liu, and Jiaya Jia. Lisa: Reasoning segmentation via large language model. In *Proceedings of the IEEE/CVF Conference on Computer Vision and Pattern Recognition*, pp. 9579–9589, 2024.

Kaiyu Li, Ruixun Liu, Xiangyong Cao, Xueru Bai, Feng Zhou, Deyu Meng, and Zhi Wang. Segearth-ov: Towards training-free open-vocabulary segmentation for remote sensing images. In *Proceedings of the Computer Vision and Pattern Recognition Conference*, pp. 10545–10556, 2025a.

Kaiyu Li, Zepeng Xin, Li Pang, Chao Pang, Yupeng Deng, Jing Yao, Guisong Xia, Deyu Meng, Zhi Wang, and Xiangyong Cao. Segearth-r1: Geospatial pixel reasoning via large language model. *arXiv preprint arXiv:2504.09644*, 2025b.

Ling Li, Yu Ye, Bingchuan Jiang, and Wei Zeng. Georeasoner: Geo-localization with reasoning in street views using a large vision-language model. In *Forty-first International Conference on Machine Learning*, 2024a.

Yansheng Li, Bo Dang, Wanchun Li, and Yongjun Zhang. Glh-water: A large-scale dataset for global surface water detection in large-size very-high-resolution satellite imagery. In *Proceedings of the AAAI Conference on Artificial Intelligence*, volume 38, pp. 22213–22221, 2024b.

Yansheng Li, Yu Wang, Lei Yu, Bo Dang, Gang Xu, Zhenyu Zhong, Yuning Wu, Xin Guo, Kang Wu, Zheng Li, et al. Learning to reason over multi-granularity knowledge graph for zero-shot urban land-use mapping. *Remote Sensing of Environment*, 330:114961, 2025c.

Haotian Liu, Chunyuan Li, Qingyang Wu, and Yong Jae Lee. Visual instruction tuning. *Advances in neural information processing systems*, 36:34892–34916, 2023a.

Qin Liu, Zhenlin Xu, Gedas Bertasius, and Marc Niethammer. Simpleclick: Interactive image segmentation with simple vision transformers. In *Proceedings of the IEEE/CVF International Conference on Computer Vision*, pp. 22290–22300, 2023b.

Yuqi Liu, Bohao Peng, Zhisheng Zhong, Zihao Yue, Fanbin Lu, Bei Yu, and Jiaya Jia. Seg-zero: Reasoning-chain guided segmentation via cognitive reinforcement. *arXiv preprint arXiv:2503.06520*, 2025a.

Yuqi Liu, Tianyuan Qu, Zhisheng Zhong, Bohao Peng, Shu Liu, Bei Yu, and Jiaya Jia. Vision-reasoner: Unified visual perception and reasoning via reinforcement learning. *arXiv preprint arXiv:2505.12081*, 2025b.

Utkarsh Mall, Cheng Perng Phoo, Meilin Kelsey Liu, Carl Vondrick, Bharath Hariharan, and Kavita Bala. Remote sensing vision-language foundation models without annotations via ground remote alignment. In *The Twelfth International Conference on Learning Representations*, 2024. URL https://openreview.net/forum?id=w9tc699w3Z.

OpenStreetMap contributors. Planet dump retrieve from https://planet.osm.org. https://www.openstreetmap.org, 2017.

Jorge E Patino and Juan C Duque. A review of regional science applications of satellite remote sensing in urban settings. *Computers, Environment and Urban Systems*, 37:1–17, 2013.

Nikhila Ravi, Valentin Gabeur, Yuan-Ting Hu, Ronghang Hu, Chaitanya Ryali, Tengyu Ma, Haitham Khedr, Roman Rädle, Chloe Rolland, Laura Gustafson, et al. Sam 2: Segment anything in images and videos. *arXiv preprint arXiv:2408.00714*, 2024.

Olaf Ronneberger, Philipp Fischer, and Thomas Brox. U-net: Convolutional networks for biomedical image segmentation. In *International Conference on Medical image computing and computer-assisted intervention*, pp. 234–241. Springer, 2015.

Zhihong Shao, Peiyi Wang, Qihao Zhu, Runxin Xu, Junxiao Song, Xiao Bi, Haowei Zhang, Mingchuan Zhang, YK Li, Yang Wu, et al. Deepseekmath: Pushing the limits of mathematical reasoning in open language models. *arXiv preprint arXiv:2402.03300*, 2024.

Chuanji Shi, Yingying Zhang, Jiaotuan Wang, Xin Guo, and Qiqi Zhu. Multimodal urban areas of interest generation via remote sensing imagery and geographical prior. *International Journal of Applied Earth Observation and Geoinformation*, 136:104326, 2025.

Jee-Young Sun, Seung-Wook Kim, Sang-Won Lee, Ye-Won Kim, and Sung-Jea Ko. Reverse and boundary attention network for road segmentation. In *Proceedings of the IEEE/CVF international conference on computer vision workshops*, pp. 0–0, 2019.

Athanasios Voulodimos, Nikolaos Doulamis, Anastasios Doulamis, and Eftychios Protopapadakis. Deep learning for computer vision: A brief review. *Computational intelligence and neuroscience*, 2018(1):7068349, 2018.

Junjue Wang, Zhuo Zheng, Ailong Ma, Xiaoyan Lu, and Yanfei Zhong. Loveda: A remote sensing land-cover dataset for domain adaptive semantic segmentation. *arXiv preprint arXiv:2110.08733*, 2021.

Weixun Wang, Shaopan Xiong, Gengru Chen, Wei Gao, Sheng Guo, Yancheng He, Ju Huang, Jiaheng Liu, Zhendong Li, Xiaoyang Li, et al. Reinforcement learning optimization for large-scale learning: An efficient and user-friendly scaling library. *arXiv preprint arXiv:2506.06122*, 2025.

Zhaoqing Wang, Yu Lu, Qiang Li, Xunqiang Tao, Yandong Guo, Mingming Gong, and Tongliang Liu. Cris: Clip-driven referring image segmentation. In *Proceedings of the IEEE/CVF conference on computer vision and pattern recognition*, pp. 11686–11695, 2022.

Fei Wei, Xinyu Zhang, Ailing Zhang, Bo Zhang, and Xiangxiang Chu. Lenna: Language enhanced reasoning detection assistant. In *ICASSP 2025-2025 IEEE International Conference on Acoustics, Speech and Signal Processing (ICASSP)*, pp. 1–5. IEEE, 2025.

Enze Xie, Wenhai Wang, Zhiding Yu, Anima Anandkumar, Jose M Alvarez, and Ping Luo. Segformer: Simple and efficient design for semantic segmentation with transformers. *Advances in neural information processing systems*, 34:12077–12090, 2021.

Shuping Xiong, Xiuyuan Zhang, Haoyu Wang, Yichen Lei, Ge Tan, and Shihong Du. Mapping the first dataset of global urban land uses with sentinel-2 imagery and poi prompt. *Remote Sensing of Environment*, 327:114824, 2025.

Xiaojun X Yang. *Urban remote sensing: monitoring, synthesis and modeling in the urban environment*. John Wiley & Sons, 2021.

Liang Yao, Fan Liu, Hongbo Lu, Chuanyi Zhang, Rui Min, Shengxiang Xu, Shimin Di, and Pai Peng. Remotereasoner: Towards unifying geospatial reasoning workflow. *arXiv preprint arXiv:2507.19280*, 2025.

Yao Yao, Xia Li, Xiaoping Liu, Penghua Liu, Zhaotang Liang, Jinbao Zhang, and Ke Mai. Sensing spatial distribution of urban land use by integrating points-of-interest and google word2vec model. *International Journal of Geographical Information Science*, 31(4):825–848, 2017.

Zijun Yao, Yanjie Fu, Bin Liu, Wangsu Hu, and Hui Xiong. Representing urban functions through zone embedding with human mobility patterns. In *Proceedings of the Twenty-Seventh International Joint Conference on Artificial Intelligence (IJCAI-18)*, 2018.

Zuyao You and Zuxuan Wu. Seg-r1: Segmentation can be surprisingly simple with reinforcement learning. *arXiv preprint arXiv:2506.22624*, 2025.

Xiuyuan Zhang, Shihong Du, and Qiao Wang. Hierarchical semantic cognition for urban functional zones with vhr satellite images and poi data. *ISPRS Journal of Photogrammetry and Remote Sensing*, 132:170–184, 2017.

Yu Zheng, Fengli Xu, Yuming Lin, Paolo Santi, Carlo Ratti, Qi R Wang, and Yong Li. Urban planning in the era of large language models. *Nature Computational Science*, pp. 1–10, 2025.

Yanfei Zhong, Bowen Yan, Jingjun Yi, Ruiyi Yang, Mengzi Xu, Yu Su, Zhendong Zheng, and Liangpei Zhang. Global urban high-resolution land-use mapping: From benchmarks to multi-megacity applications. *Remote Sensing of Environment*, 298:113758, 2023.

Qi Zhu, Jiangwei Lao, Deyi Ji, Junwei Luo, Kang Wu, Yingying Zhang, Lixiang Ru, Jian Wang, Jingdong Chen, Ming Yang, et al. Skysense-o: Towards open-world remote sensing interpretation with vision-centric visual-language modeling. In *Proceedings of the Computer Vision and Pattern Recognition Conference*, pp. 14733–14744, 2025.

Chengke Zou, Xingang Guo, Rui Yang, Junyu Zhang, Bin Hu, and Huan Zhang. Dynamath: A dynamic visual benchmark for evaluating mathematical reasoning robustness of vision language models. *arXiv preprint arXiv:2411.00836*, 2024.

A Appendix

A.1 Dataset Details

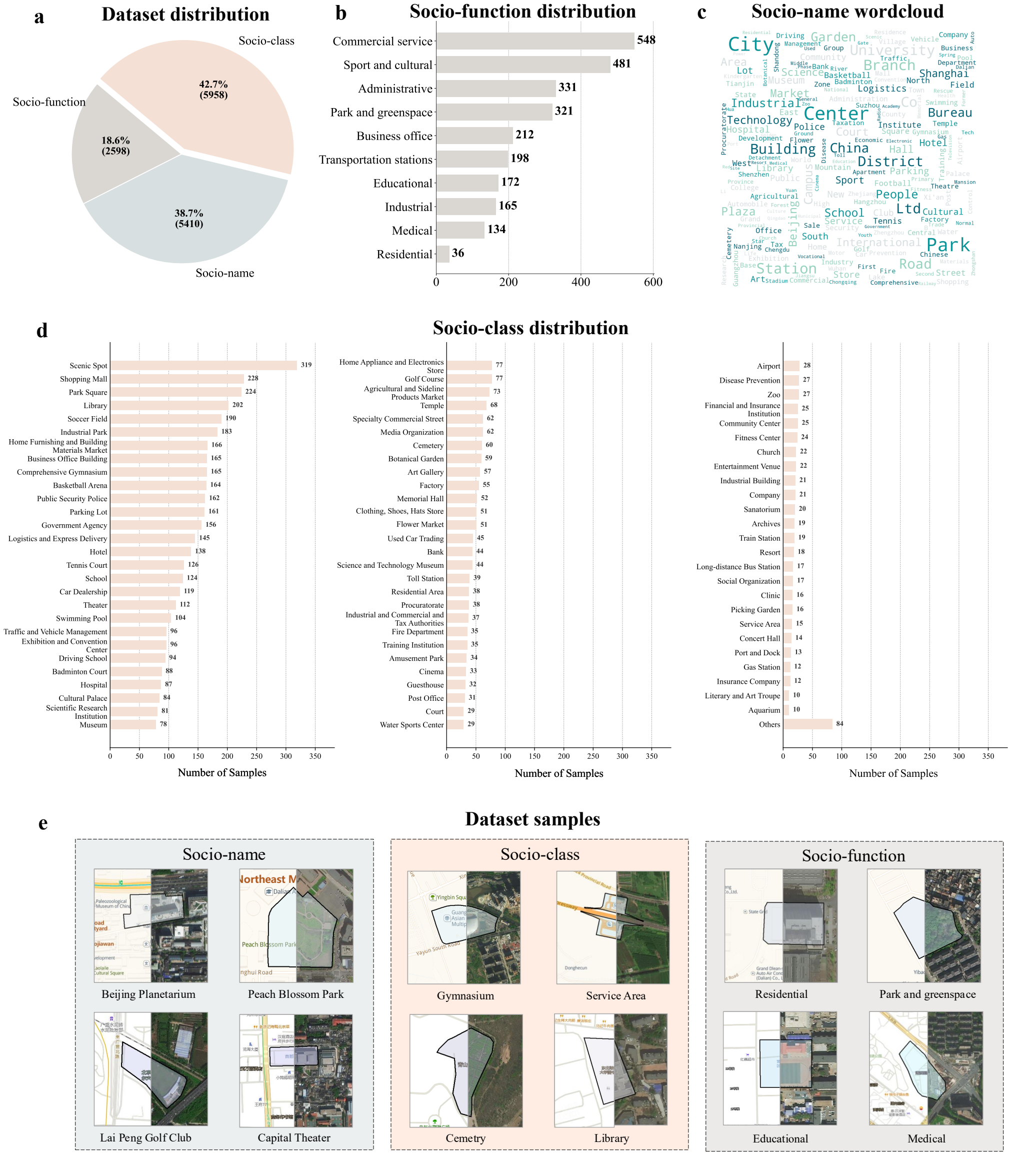

Figure 6: The SocioSeg dataset overview. (a) Sample distribution across the three hierarchical tasks. (b) Socio-function class distribution. (c) Socio-name word cloud. (d) Socio-class distribution. (e) Sample examples from SocioSeg, including satellite images, digital maps, and socio-semantic mask labels.

A.1.1 SocioSeg Dataset

The SocioSeg dataset is constructed entirely from data provided by Amap, offering comprehensive geographic coverage of all provinces and major cities across China. The input modalities, namely satellite images and digital maps, are acquired via the public Amap API. The ground-truth labels are derived from Amap's Area of Interest (AOI) data.

To clarify the semantic scope, we structure these labels into three hierarchical levels intrinsically linked to daily social activities: the **Socio-Name** level corresponds to the specific name of each AOI instance; the **Socio-Class** level adopts the standard third-level POI taxonomy from Amap, a classification widely utilized in prior studies (Hu & Han, 2019; Yao et al., 2017); and the **Socio-Function** level is derived from established urban functional zone definitions (Gong et al., 2020; Li et al., 2025c).

To adapt this source data for our research, we performed several refinement steps, encompassing reformatting the vector-based AOI data into rasterized semantic masks and conducting a rigorous quality assurance process. Specifically, we manually verified the alignment between the AOI polygons and the actual physical boundaries, rigorously filtering the dataset from an initial pool of approximately 40,000 samples down to 13,000 to exclude misaligned or ambiguous annotations. To further quantify the annotation quality and reproducibility, we conducted an inter-annotator agreement study with three independent annotators on a random subset of 500 samples, yielding a Cohen's Kappa coefficient of 0.854. This ensures that each pixel is precisely classified into its corresponding socio-functional category, enhancing the dataset's overall fidelity and reliability. The resulting SocioSeg benchmark is thus rich in socio-semantic information, providing a robust foundation for urban socio-semantic segmentation research.

Figure 6 offers a comprehensive overview of the SocioSeg dataset. Specifically, subfigure (a) illustrates the sample distribution across the three hierarchical tasks, underscoring the dataset's balance and diversity. Subfigures (b) and (d) present the class distributions for the socio-function and socio-class tasks, respectively, showcasing the variety of categories included. A word cloud in subfigure (c) visualizes the frequency and prominence of the socio-name labels. Finally, subfigure (e) provides qualitative examples from the dataset, displaying corresponding satellite images, digital maps, and socio-semantic masks that effectively demonstrate the data's richness and complexity.

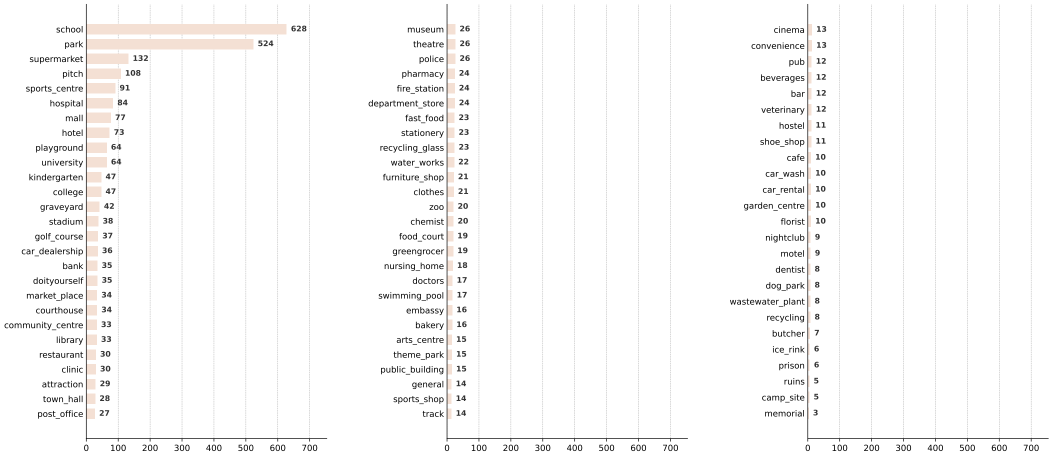

Figure 7: The SocioSeg OOD (New Region) dataset distribution.

A.1.2 SocioSeg Out-Of-Distribution dataset

To rigorously evaluate the generalization capabilities of our model, we introduce two distinct Out-Of-Distribution (OOD) datasets: **Map Style** and **New Region**.

OOD (Map Style). This setting is designed to assess the model's robustness to shifts in cartographic rendering and symbolization. We utilize the original test set from the SocioSeg benchmark, retaining the original satellite imagery and ground-truth labels. However, we replace the input digital map modality, originally sourced from Amap, with tiles fetched from Google Maps. This substitution isolates the impact of map style, requiring the model to generalize to a new cartographic domain without any fine-tuning.

OOD (New Region). Figure 7 shows the distribution of the SocioSeg OOD (New Region) dataset. This setting evaluates performance across diverse geographic environments. We constructed this dataset using OpenStreetMap (OSM) (OpenStreetMap contributors, 2017) AOI data, strictly adhering to the same data construction and quality assurance pipeline employed for the primary SocioSeg dataset. To ensure global diversity, we selected five representative cities from different continents: Tokyo (Asia), New York (North America), São Paulo (South America), London (Europe), and Nairobi (Africa). While the input digital maps are sourced from Google Maps, the ground truth labels were derived from OSM and underwent manual filtering to ensure high fidelity. The resulting dataset comprises 3,200 samples focused on the socio-class task. It encompasses 80 distinct categories, importantly including 24 novel categories that were not present in the training set, thereby posing a significant challenge for zero-shot generalization.

Algorithm 1 Two-stage end-to-end GRPO Training for SocioReasoner

```
Require: Training dataset $\mathcal{D}_{\text{train}}$; VLM policy $\pi_\theta$; frozen SAM $\mathcal{S}$; renderer $\mathcal{D}$; reference policy
    $\pi_{\text{ref}}$; group size $G$; PPO clip $\epsilon$; KL weight $\beta$; optimizer with learning rate $\eta$; number of RL
    steps $T$
Initialize $\pi_{\theta_{\text{old}}} \leftarrow \pi_\theta$
for step $= 1$ to $T$ do
    Sample a mini-batch $\mathcal{B} \subset \mathcal{D}_{\text{train}}$
    for all $(\mathbf{I}_s, \mathbf{I}_m, \mathbf{t}_b) \in \mathcal{B}$ do
        $\mathbf{x}_1 \leftarrow (\mathbf{I}_s, \mathbf{I}_m, \mathbf{t}_b)$                                    ▷ Stage-1: Localization
        for $g = 1$ to $G$ do
            Sample completion $\mathbf{y}_1^{(g)} \sim \pi_\theta(\cdot \mid \mathbf{x}_1)$
            Parse bounding boxes $\mathcal{B}^{(g)}$ from $\mathbf{y}_1^{(g)}$ (assign syntax reward 0 if invalid)
            $\mathbf{M}_c^{(g)} \leftarrow \mathcal{S}(\mathbf{I}_s, \text{prompt} = \mathcal{B}^{(g)})$
            Compute $R_1^{(g)}$
        end for
        $b_1 \leftarrow \frac{1}{G} \sum_{g=1}^{G} R_1^{(g)}$
        Compute advantages $A_1^{(g)} \leftarrow R_1^{(g)} - b_1$ for all $g$
        Update policy $\pi_\theta$ with GRPO on $\{\mathbf{x}_1, \mathbf{y}_1^{(g)}, A_1^{(g)}\}_{g=1}^{G}$, using clip $\epsilon$ and KL weight $\beta$
        Select $g^\star \leftarrow \arg\max_g R_1^{(g)}$ (or sample proportional to $\exp(R_1^{(g)})$)
        $\mathbf{I}_{s,r} \leftarrow \mathcal{D}(\mathbf{I}_s, \mathcal{B}^{(g^\star)}, \mathbf{M}_c^{(g^\star)})$
        $\mathbf{I}_{m,r} \leftarrow \mathcal{D}(\mathbf{I}_m, \mathcal{B}^{(g^\star)}, \mathbf{M}_c^{(g^\star)})$
        $\mathbf{x}_2 \leftarrow (\mathbf{I}_{s,r}, \mathbf{I}_{m,r}, \mathbf{t}_b, \mathbf{M}_c^{(g^\star)})$                ▷ Stage-2: Refinement
        for $g = 1$ to $G$ do
            Sample completion $\mathbf{y}_2^{(g)} \sim \pi_\theta(\cdot \mid \mathbf{x}_2)$
            Parse $\{\tilde{\mathcal{B}}^{(g)}, \mathcal{P}^{(g)}\}$ from $\mathbf{y}_2^{(g)}$ (assign syntax reward 0 if invalid)
            $\mathbf{M}_f^{(g)} \leftarrow \mathcal{S}(\mathbf{I}_s, \text{prompt} = \{\tilde{\mathcal{B}}^{(g)}, \mathcal{P}^{(g)}\})$
            Compute $R_2^{(g)}$
        end for
        $b_2 \leftarrow \frac{1}{G} \sum_{g=1}^{G} R_2^{(g)}$
        Compute advantages $A_2^{(g)} \leftarrow R_2^{(g)} - b_2$ for all $g$
        Update policy $\pi_\theta$ with GRPO on $\{\mathbf{x}_2, \mathbf{y}_2^{(g)}, A_2^{(g)}\}_{g=1}^{G}$, using clip $\epsilon$ and KL weight $\beta$
    end for
    $\pi_{\theta_{\text{old}}} \leftarrow \pi_\theta$                                    ▷ Refresh behavior policy for next step
end for
```

A.2 Implementation Details

A.2.1 GRPO Optimization Details

We train SocioReasoner with the two-stage end-to-end GRPO algorithm. The training process is summarized in Algorithm 1. In contrast to the single-stage training of existing methods, SocioReasoner's process includes two rounds of RL sampling and policy updates, all while utilizing a shared set of model parameters.

A.2.2 Reward Function Design

Format Reward Functions. The policy generates a structured textual output $\mathbf{y}$ containing a free-form reasoning channel and a machine-parsable answer channel:

$$\langle\texttt{think}\rangle \ \ldots \ \langle\texttt{/think}\rangle \quad \langle\texttt{answer}\rangle \ \texttt{JSON} \ \langle\texttt{/answer}\rangle.$$

The answer channel must contain a valid JSON array of objects. In stage-1, each object specifies a bounding box: {"bbox_2d": [x1,y1,x2,y2]}. In stage-2, each object is augmented with a list of points: {"bbox_2d": [...], "points": [[x,y], ...]}. We define a binary format reward, $R_{\text{form}}(\mathbf{y}) \in \{0, 1\}$, which is 1 if and only if the output is syntactically correct and adheres to the stage-specific schema. If the format reward is 0, the total reward for the episode is also 0, overriding all other components.

Stage-1 (Localization) Reward. Given the ground-truth set of boxes $\mathcal{B}^\star = \{\mathbf{b}_j^\star\}_{j=1}^J$ and the predicted set $\hat{\mathcal{B}} = \{\hat{\mathbf{b}}_k\}_{k=1}^K$, we define:

- **Format reward** $R_{\text{form}}^{(1)}(\mathbf{y})$ as defined above.
- **Accuracy reward** via Hungarian matching with an IoU threshold of 0.5. Let $\text{IoU}(\mathbf{b}, \mathbf{b}')$ be the standard box IoU. We form a binary match matrix $\mathbf{M}_{k,j} = \mathbf{1}(\text{IoU}(\hat{\mathbf{b}}_k, \mathbf{b}_j^\star) > 0.5)$, solve the linear assignment problem on the cost matrix $\mathbf{1} - \mathbf{M}$, and denote the number of matches as N_m. The accuracy reward is

$$R_{\text{acc}}^{(1)}(\mathbf{y}; \mathcal{B}^\star) = \frac{N_m}{\max(K, J)} \ \in \ [0, 1]. \tag{7}$$

- **Length reward** that encourages predicting the correct number of instances:

$$R_{\text{len}}^{(1)}(\mathbf{y}; \mathcal{B}^\star) = \exp\big(-2\,|K - J|/J\big), \quad J > 0. \tag{8}$$

The total stage-1 reward is the unweighted sum of these components:

$$R_1(\mathbf{y}; \mathbf{x}) = R_{\text{form}}^{(1)}(\mathbf{y}) + R_{\text{acc}}^{(1)}(\mathbf{y}; \mathcal{B}^\star) + R_{\text{len}}^{(1)}(\mathbf{y}; \mathcal{B}^\star). \tag{9}$$

Stage-2 (Refinement) Reward. For each predicted group (one bbox plus its point list), we execute SAM with the prompts to obtain a mask $\hat{\mathbf{M}}_f$ and compare it to the ground-truth mask $\mathbf{M}^\star$:

- **Format reward** $R_{\text{form}}^{(2)}(\mathbf{y})$ as defined above.
- **Accuracy reward** as pixel IoU:

$$R_{\text{acc}}^{(2)}(\mathbf{y}; \mathbf{x}) = \text{IoU}(\hat{\mathbf{M}}_f, \mathbf{M}^\star) \ \in \ [0, 1]. \tag{10}$$

- **Length reward** that encourages concise, informative interactions. For a group with n points, we define a Gaussian-shaped score peaking at two points:

$$R_{\text{len}}^{(2)}(\mathbf{y}) = \frac{1}{G'} \sum_{g=1}^{G'} r(n) \ \in \ [0, 1], \tag{11}$$

where $r(n) = \exp\big(-\frac{(n-\mu)^2}{2\sigma^2}\big)$ with $\mu = 2$ and $\sigma = 2$. G' is the number of valid groups. This encourages using a small number of informative points rather than many redundant ones.

The total stage-2 reward is the sum of these components:

$$R_2(\mathbf{y}; \mathbf{x}) = R_{\text{form}}^{(2)}(\mathbf{y}) + R_{\text{acc}}^{(2)}(\mathbf{y}; \mathbf{x}) + R_{\text{len}}^{(2)}(\mathbf{y}). \tag{12}$$

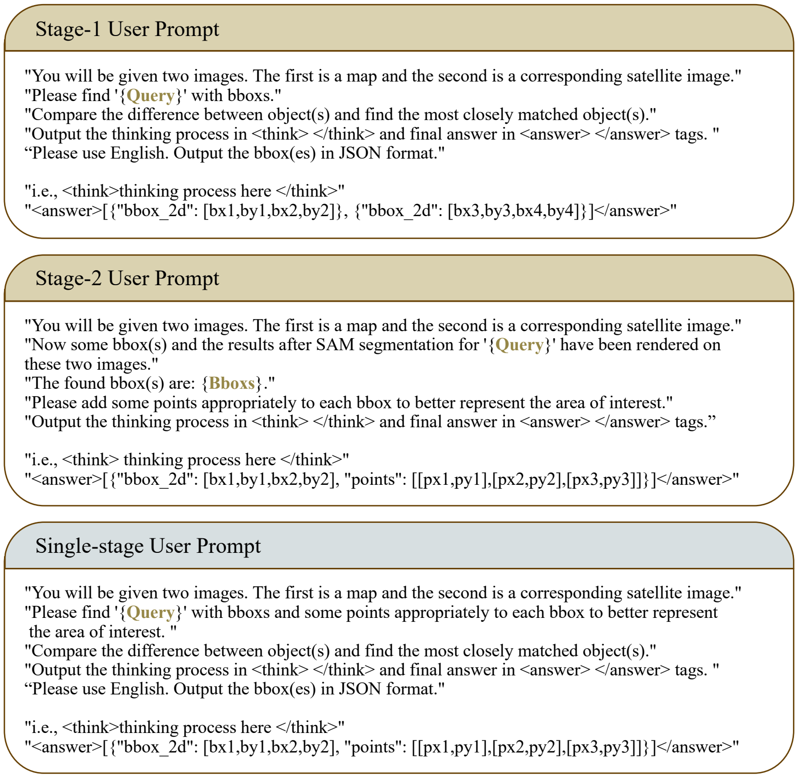

Stage-1 User Prompt

"You will be given two images. The first is a map and the second is a corresponding satellite image."
"Please find '{**Query**}' with bboxs."
"Compare the difference between object(s) and find the most closely matched object(s)."
"Output the thinking process in <think> </think> and final answer in <answer> </answer> tags. "
“Please use English. Output the bbox(es) in JSON format."

"i.e., <think>thinking process here </think>"
"<answer>[{"bbox_2d": [bx1,by1,bx2,by2]}, {"bbox_2d": [bx3,by3,bx4,by4]}]</answer>"

Stage-2 User Prompt

"You will be given two images. The first is a map and the second is a corresponding satellite image."
"Now some bbox(s) and the results after SAM segmentation for '{**Query**}' have been rendered on these two images."
"The found bbox(s) are: {**Bboxs**}."
"Please add some points appropriately to each bbox to better represent the area of interest."
"Output the thinking process in <think> </think> and final answer in <answer> </answer> tags.”

"i.e., <think> thinking process here </think>"
"<answer>[{"bbox_2d": [bx1,by1,bx2,by2], "points": [[px1,py1],[px2,py2],[px3,py3]]}]</answer>"

Single-stage User Prompt

"You will be given two images. The first is a map and the second is a corresponding satellite image."
"Please find '{**Query**}' with bboxs and some points appropriately to each bbox to better represent the area of interest. "
"Compare the difference between object(s) and find the most closely matched object(s)."
"Output the thinking process in <think> </think> and final answer in <answer> </answer> tags. "
“Please use English. Output the bbox(es) in JSON format."

"i.e., <think>thinking process here </think>"
"<answer>[{"bbox_2d": [bx1,by1,bx2,by2], "points": [[px1,py1],[px2,py2],[px3,py3]]}]</answer>"

Figure 8: The two prompts above are the user prompt template for SocioReasoner, which adopts a two-stage reasoning process to mimic human annotation. The prompt below is the single-stage prompt used for the baseline without reflection and zero-shot GPT and Qwen models.

A.2.3 Experimental Settings

For all our Reinforcement Learning (RL) based models, namely VisionReasoner, Seg-R1, SAM-R1, and RemoteReasoner, we adopt a unified training configuration. We set the rollout batch size to 128 and the group size to 8. The models are optimized using the AdamW optimizer with a learning rate of 1×10^{-6}. For the Proximal Policy Optimization (PPO) algorithm, the clipping parameter ϵ is set to 0.5, and the Kullback-Leibler (KL) divergence weight β is configured to 0.005. All RL models are trained for 250 steps within the ROLL framework (Wang et al., 2025).

A key aspect of our methodology is the handling of visual inputs. Since all RL-based methods are built upon Qwen2.5-VL-3b, which natively supports multi-image inputs, we provide both the satellite imagery and digital maps as visual input. For the Supervised Fine-Tuning (SFT) version of our model, we construct the supervision signal using the bounding box of the ground-truth mask, along with three points randomly sampled from within the mask's area.

In contrast, for the baseline models UNet, SegFormer, SegEarth-OV, RSRefSeg and SegEarth-R1, we followed the original authors' implementations. We utilized their publicly available source code and pre-trained models, which are then fine-tuned on the SocioSeg dataset. As these architectures do not support multi-image inputs, only the satellite imagery is used as the visual input for these models. All models are trained on a high-performance computing cluster equipped with 16 NVIDIA H20 GPUs.

A.3 User Prompt Template

The user prompt templates utilized in our experiments are shown in Figure 8. SocioReasoner employs a two-stage reasoning process; consequently, we designed two distinct prompt templates to accommodate the different input and output formats of each stage. For our baseline model without

Table 5: All ablation of multi-stage.

Method	Socio-name			Socio-class			Socio-function			All dataset		
	cIoU	gIoU	F1	cIoU	gIoU	F1	cIoU	gIoU	F1	cIoU	gIoU	F1
w/o reflection	48.5	50.9	58.4	44.4	49.3	55.5	36.3	41.8	45.0	44.0	48.5	54.3
w/o refinement	50.5	53.1	61.2	46.2	51.0	58.1	40.3	45.7	48.1	46.4	50.8	57.5
Ours	**52.6**	**55.7**	**64.6**	**47.6**	**52.8**	**60.1**	**40.6**	**46.9**	**50.3**	**47.9**	**52.8**	**59.7**

Table 6: All ablation of point number.

Method	Socio-name			Socio-class			Socio-function			All dataset		
	cIoU	gIoU	F1	cIoU	gIoU	F1	cIoU	gIoU	F1	cIoU	gIoU	F1
1 point refinement	51.6	53.4	61.2	47.6	51.2	59.0	40.0	45.7	49.5	47.6	51.2	58.0
2 points refinement	52.6	**55.7**	64.6	47.6	**52.8**	**60.1**	40.6	**46.9**	**50.3**	47.9	**52.8**	**59.7**
3 points refinement	**53.2**	54.7	**65.0**	**48.9**	52.6	59.7	**41.8**	46.6	49.8	**48.9**	52.3	58.8

the reflection mechanism, as well as the GPT and Qwen models, we adopt a single-stage prompt template. This template is adapted from the one used by VisionReasoner, with modifications to meet the specific requirements of our task. For our SFT model, we use this same base template but remove the chain-of-thought components. For all other RL-based comparative methods, we used the original prompt templates provided by their respective authors, prepending each with the instruction, ”You will be given two images. The first is a map and the second is a corresponding satellite image.”

Table 7: Comparison with state-of-the-art methods on the SocioSeg OOD (New Region) dataset.

Method	OOD (New Region) Dataset		
	cIoU	gIoU	F1
UNet	10.0	7.3	7.1
Segformer	18.8	14.7	14.1
VisionReasoner	32.8	34.4	35.0
Seg-R1	28.8	28.8	26.2
SAM-R1	14.8	14.5	19.0
SegEarth-OV	3.2	3.2	0.0
RSRefSeg	12.4	10.3	13.8
SegEarth-R1	20.7	18.7	21.2
RemoteReasoner	27.5	29.8	28.1
Ours	**40.2**	**43.4**	**42.9**

A.4 SocioSeg benchmark

GPT-5, GPT-o3 and Qwen2.5-VL-72b are evaluated as baselines without any fine-tuning. As shown in Table 9, their performance is substantially lower than that of our trained model, indicating that even large-scale VLMs struggle with the complexities of socio-semantic segmentation without task-specific training. Notably, Qwen2.5-VL-3b fails to produce valid bounding box outputs in our experiments, resulting in zero performance. This underscores the importance of specialized training and the effectiveness of our reinforcement learning approach in eliciting the reasoning capabilities necessary for this task.

A.5 More Quantitative Results

A.5.1 Per-Category Results

We present the comprehensive accuracy metrics for all socio-class and socio-function categories in Figure 13 and Figure 14, respectively. While our method consistently outperforms baselines on the top-20 most frequent socio-class categories, it exhibits suboptimal performance in specific

Table 8: Inference time comparison (seconds per sample).

VisionReasoner	Seg-R1	SAM-R1	RSRefSeg	SegEarth-R1	RemoteReasoner	Ours(rl)	Ours(sft)
1.33	1.07	2.52	0.16	0.35	1.13	2.71	0.41

Table 9: SocioSeg benchmark.

Method	Backbone	Socio-name		Socio-class		Socio-function		All dataset	
		cIoU	gIoU	cIoU	gIoU	cIoU	gIoU	cIoU	gIoU
GPT-5	Not disclosed	16.1	16.1	14.9	15.1	12.2	12.5	14.7	15.0
GPT-o3	Not disclosed	22.6	22.9	20.9	22.7	16.1	17.3	20.3	21.7
Qwen2.5-VL-3b	Qwen2.5-VL-3b	0.0	0.0	0.0	0.0	0.0	0.0	0.0	0.0
Qwen2.5-VL-72b	Qwen2.5-VL-72b	27.1	29.5	21.8	27.2	20.4	24.4	23.1	27.5

classes such as *Training Institution* and *Badminton Court*. Regarding the socio-function tasks, our approach achieves state-of-the-art results across all categories, with the exception of *Business Office* and *Residential*. We attribute these failures to error propagation: in certain samples, the initial bounding box localization (Stage-1) deviates significantly from the ground truth. Consequently, the point prompts generated during the refinement phase (Stage-2) tend to exacerbate rather than correct this initial deviation, as illustrated in the failure cases in Figure 11.

A.5.2 More Ablation Studies and Inference Time Comparison

We provide the comprehensive quantitative results of our ablation studies in Table 5 and Table 6, presenting detailed metrics across all three hierarchical task levels. Furthermore, Table 5 reports the performance of all comparative methods on the OOD (New Region) dataset, demonstrating that our method consistently achieves the best results across all evaluation metrics. Finally, we present a computational efficiency analysis in Table 8, comparing the average inference time per sample (in seconds) against the baselines. While our model incurs a higher latency due to its iterative two-stage reasoning mechanism, this computational trade-off is justified by its superior segmentation accuracy.

A.6 More Visualizations

We first present the trend of the reward function during the training process, as shown in Figure 9. As can be seen, the reward function gradually converges as training progresses, indicating that the model continuously improves its decision-making quality. Next, we provide additional qualitative results comparing SocioReasoner's performance on the three hierarchical tasks, as illustrated in Figure 10. These examples clearly demonstrate the advantages of SocioReasoner's performance across different tasks, especially its accuracy and robustness in complex scenarios. Furthermore, we showcase more inference examples from SocioReasoner in Figure 12. These examples further validate SocioReasoner's capability in processing multi-modal inputs.

A.7 Failure Cases

Finally, we present a visualization of representative failure cases encountered by SocioReasoner in Figure 11. These instances, all characterized by a Generalized IoU (gIoU) below 0.1, primarily stem from two distinct error modes: (i) Localization Failure (Cases 1 and 2), where the predicted bounding box fails to locate the target region entirely, likely due to the model being distracted by the dense and visually cluttered urban environment; and (ii) Boundary Imprecision (Cases 3, 4, and 5), where the model correctly identifies the general location of the semantic entity but fails to generate a geometrically accurate enclosure. These challenges underscore the inherent difficulty of mapping abstract social concepts to precise physical coordinates in complex satellite imagery. This suggests that while our reasoning framework effectively bridges the modal gap, future research should further focus on enhancing the fine-grained spatial reasoning capabilities of Vision-Language Models (VLMs) and mitigating spatial ambiguity to achieve more robust performance in dense urban scenarios.

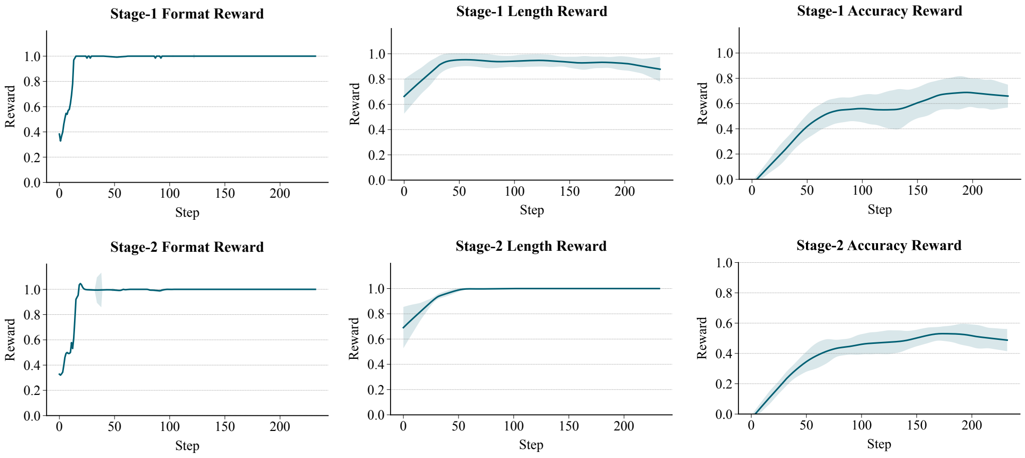

Figure 9: The rewards visualization during the training process.

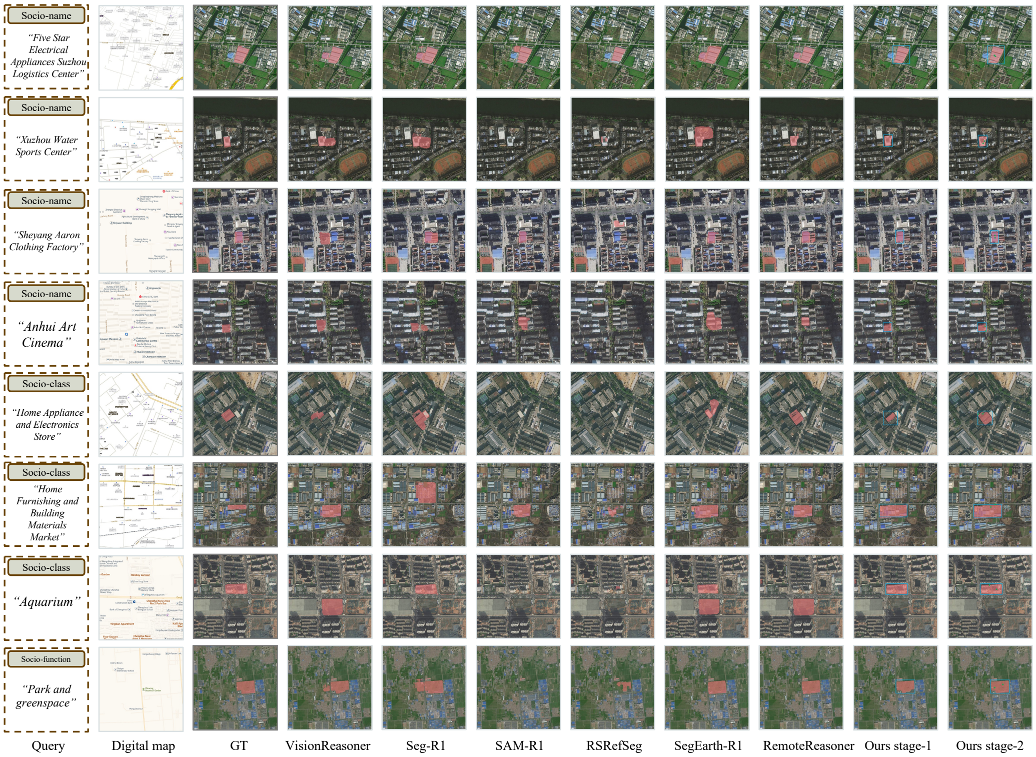

Figure 10: All method Comparisons of SocioReasoner across the three hierarchical tasks.

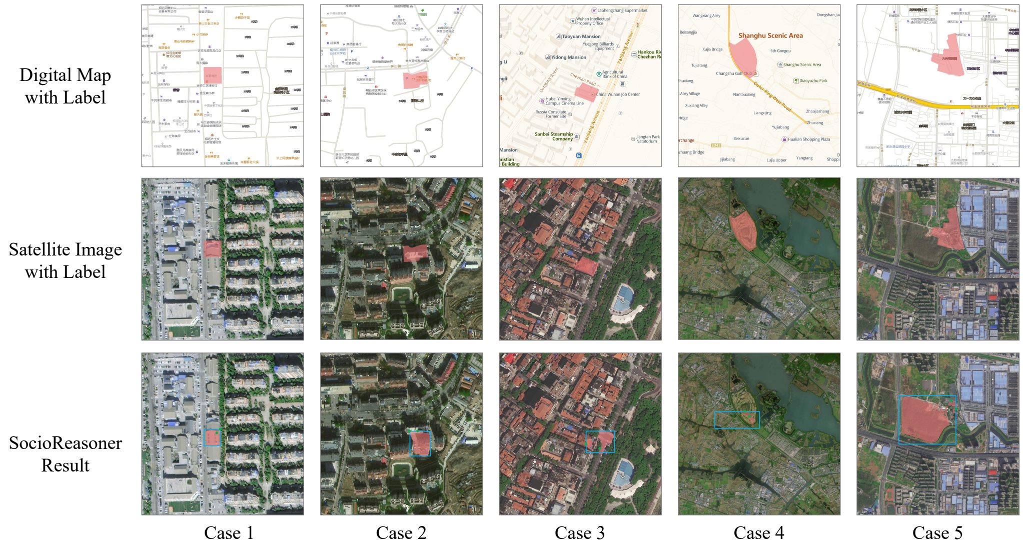

Figure 11: Failure cases of SocioReasoner.

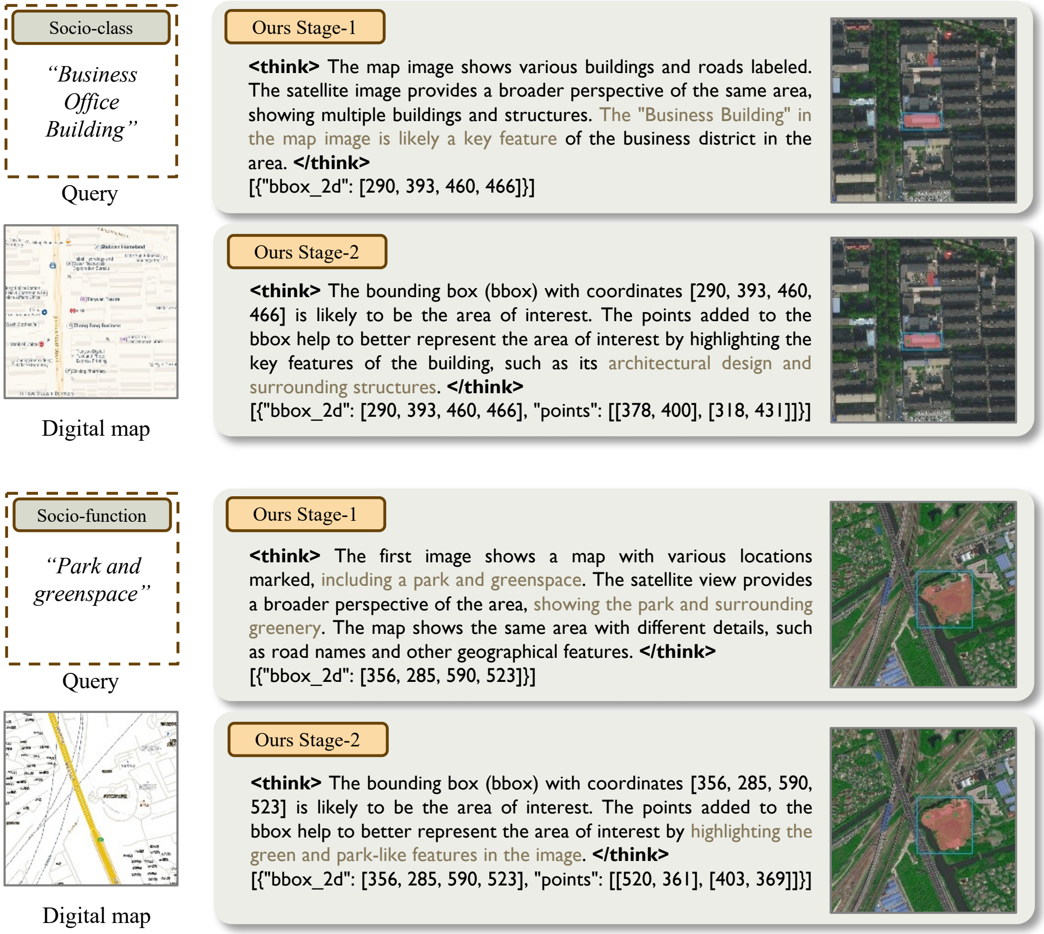

Ours Stage-1

<think> The map image shows various buildings and roads labeled. The satellite image provides a broader perspective of the same area, showing multiple buildings and structures. The "Business Building" in the map image is likely a key feature of the business district in the area. </think>
[{"bbox_2d": [290, 393, 460, 466]}]

Ours Stage-2

<think> The bounding box (bbox) with coordinates [290, 393, 460, 466] is likely to be the area of interest. The points added to the bbox help to better represent the area of interest by highlighting the key features of the building, such as its architectural design and surrounding structures. </think>
[{"bbox_2d": [290, 393, 460, 466], "points": [[378, 400], [318, 431]]}]

Ours Stage-1

<think> The first image shows a map with various locations marked, including a park and greenspace. The satellite view provides a broader perspective of the area, showing the park and surrounding greenery. The map shows the same area with different details, such as road names and other geographical features. </think>
[{"bbox_2d": [356, 285, 590, 523]}]

Ours Stage-2

<think> The bounding box (bbox) with coordinates [356, 285, 590, 523] is likely to be the area of interest. The points added to the bbox help to better represent the area of interest by highlighting the green and park-like features in the image. </think>
[{"bbox_2d": [356, 285, 590, 523], "points": [[520, 361], [403, 369]]}]

Figure 12: More inference examples of SocioReasoner.

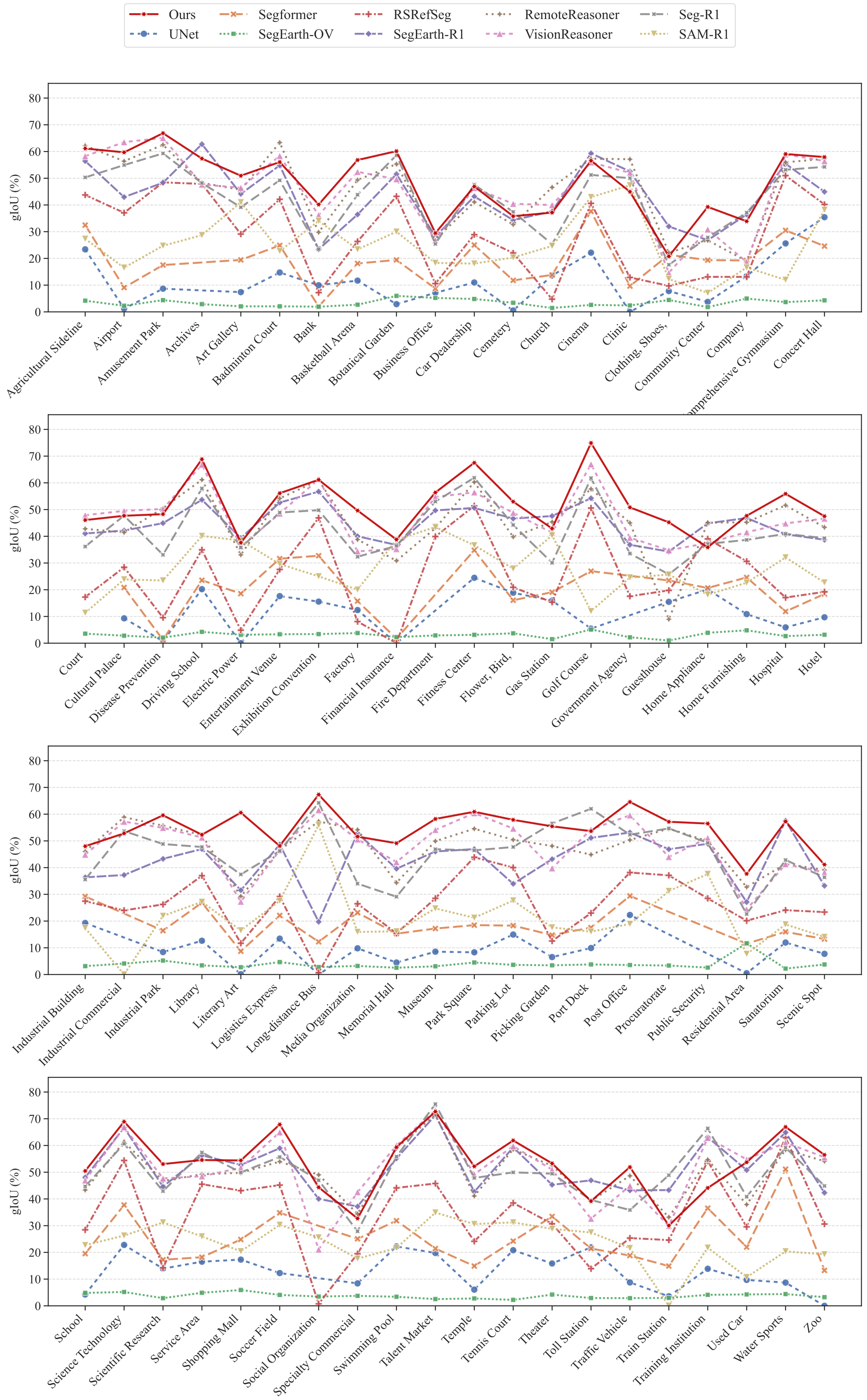

Figure 13: Per-class accuracy comparison across Socio-classes.

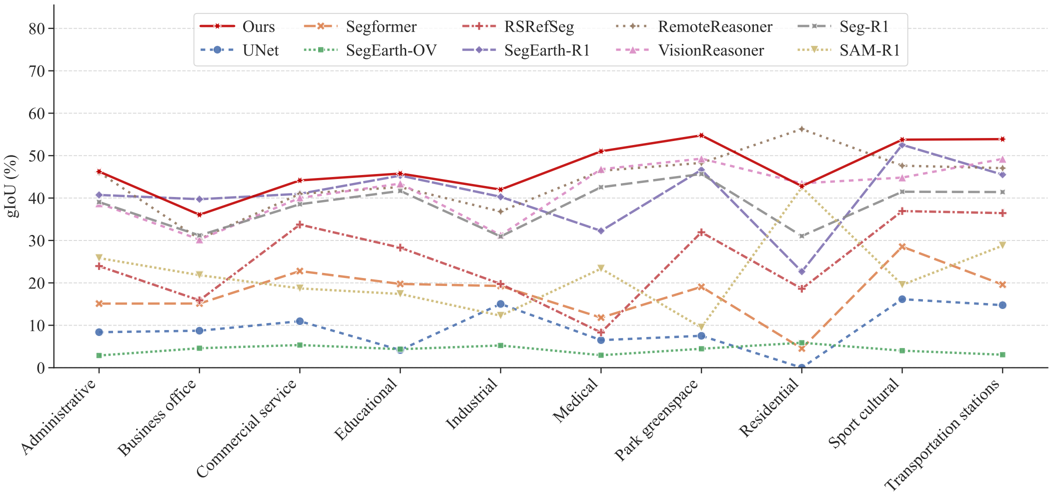

Figure 14: Per-class accuracy comparison across Socio-functions.